Macromolecules

Article

Polymerization-Induced Self-Assembly of All-Acrylic Diblock Copolymers via RAFT Dispersion Polymerization in Alkanes

Liam P. D. Ratcliffe,[†] Beulah E. McKenzie,[†] Gaëlle M. D. Le Bouëdec,[†] Clive N. Williams,[‡] Steven L. Brown,[‡] and Steven P. Armes*[,†]

[†]Dainton Building, Department of Chemistry, The University of Sheffield, Brook Hill, Sheffield, South Yorkshire S3 7HF, U.K.
[‡]Scott Bader Company Ltd., Wollaston, Wellingborough, Northants NN29 7RL, U.K.

Ⓢ Supporting Information

ABSTRACT: A series of all-acrylic poly(lauryl acrylate)−poly(benzyl acrylate) (PLA−PBzA) diblock copolymer nanoparticles are prepared by reversible addition−fragmentation chain transfer (RAFT) dispersion polymerization of benzyl acrylate in *n*-heptane, *n*-dodecane, or isohexadecane. As the PBzA block grows from the soluble PLA block it eventually becomes insoluble, which drives *in situ* polymerization-induced self-assembly (PISA). High monomer conversions (>99%) can be achieved and high blocking efficiencies are observed using ^{1}H NMR spectroscopy and gel permeation chromatography, respectively. However, final M_w/M_n values range from 1.36 to 2.10, which suggests that chain transfer to polymer occurs in these all-acrylic PISA formulations. The soft, film-forming nature of these all-acrylic nanoparticles makes conventional TEM studies problematic. However, inspecting the visual appearance of these dispersions combined with DLS studies allows the construction of a phase diagram, which has been validated by cryo-TEM studies of selected copolymers. The latter technique confirms that spherical, worm-like or vesicular morphologies can be obtained depending on the copolymer concentration, mean degree of polymerization of the core and stabilizer blocks, and choice of solvent. Oscillatory rheology studies indicate that PLA−PBzA worms form free-standing worm gels at 20 °C with relatively low moduli ($G' \sim 20$ Pa). Moreover, reversible thermal transitions are observed below ~15 °C and above ~67 °C. Finally, worm gels that exhibit critical gelation concentrations as low as 2.5% w/w at 20 °C can be prepared at up to 40% w/w solids using a convenient one-pot protocol. In summary, this new PISA formulation represents a cost-effective, facile synthesis route to all-acrylic nano-objects in non-polar solvents.

All-acrylic RAFT PISA formulation in alkanes
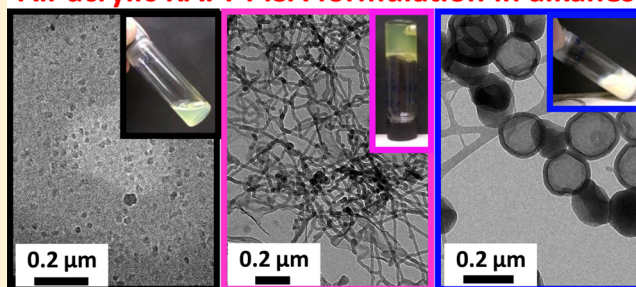
INTRODUCTION

Traditionally, dispersion polymerization has provided a facile route to well-defined, colloidally stable latexes in non-polar solvents via addition of a suitable steric stabilizer—usually an adsorbed homopolymer, block copolymer, or graft copolymer.[1] In contrast to emulsion polymerization, the monomer is soluble in the solvent and the initial reaction mixture is homogeneous: polymerization leads to the formation of an *insoluble* polymer, which leads to nucleation and ultimately to sterically stabilized latex particles (usually in the 0.1−10 μm size range).[2−6] Dispersion polymerization was originally developed for paints and coatings applications,[7] but the relatively narrow particle size distributions[8,9] led to a broader range of applications ranging from biomedical assays to particulate modeling.[7,10−13] It is well-known that AB diblock copolymers can self-assemble to form micelles in a solvent that is selective for one of the blocks.[14−24] A wide range of copolymer morphologies are known,[25] but post-polymerization processing (such as a solvent or pH switch,[26] thin film rehydration,[27−29] or electroformation[30]) is usually required, with this additional step normally being conducted at relatively high dilution (typically <5% solids).

The development of controlled radical polymerization (CRP) techniques such as nitroxide-mediated polymerization (NMP),[31,51], atom transfer radical polymerization (ATRP),[32,33] or reversible addition-fragmentation chain transfer (RAFT)[34] has led to the synthesis of many well-defined, functional block copolymers over the past two decades.[35−45] By utilizing the latter technique in a suitable selective solvent, a wide range of diblock copolymer nano-objects can be formed directly *in situ* at high copolymer concentrations (up to 50% solids) by polymerization-induced self-assembly (PISA).[46,47] The copolymer morphology is dictated by the relative volume fractions of each block, with spheres, worms or vesicles being obtained as the proportion of the core-forming block is gradually increased.[25,47] Various potential applications have been explored,[25,48−51] and this efficient new approach has sparked renewed interest in conducting dispersion polymerizations in non-polar solvents, which may be useful in areas such as inkjet printing or electronic displays.[52]

Many PISA syntheses are described in the literature: such formulations are commonly conducted via emulsion[53−60] or dispersion polymerization in either aqueous[61−71] or alcoholic media.[42,72−88] However, there are rather few examples of PISA syntheses in non-polar media. Early examples include poly(4-vinylpyridine)−polystyrene diblock copolymers prepared in cyclohexane[89] and poly(styrene-*alt*-maleic anhydride)-based copolymers in chloroform.[90] More recently, Armes and co-workers reported the preparation of a series of poly(lauryl methacrylate)−poly(benzyl methacrylate) (PLMA−PBzMA) diblock copolymers in *n*-heptane.[91] A detailed phase diagram was constructed, which proved to be essential for the reproducible targeting of spherical, worm-like, or vesicular morphologies. Interestingly, PLMA−PBzMA worms undergo a worm-to-sphere transition on heating, which leads to *in situ* degelation.[92] This is complementary behavior to that reported previously for aqueous methacrylic copolymer worms, which undergo a worm-to-sphere transition on cooling to sub-ambient temperatures.[93] Subsequently, Pei et al. reported similar thermoresponsive behavior for poly(stearyl methacrylate)−poly(3-phenylpropyl methacrylate) prepared in *n*-tetradecane as well as related copolymers in alcoholic media.[94] In each case, surface plasticization of the worms by solvent molecules drives the morphological transition.

Despite the growing interest in RAFT-mediated PISA, there have been very few studies of all-acrylic formulations. This is perhaps surprising since, along with methacrylates and styrenes, acrylates have historically been among the most important monomer classes, especially for dispersion polymerization in non-polar solvents.[7] Poly(acrylates) have lower glass transition temperature (T_g) values than their methacrylate counterparts and hence are useful for the production of polymeric films[95] and adhesives[96] at lower temperatures. A range of applications are being explored for self-assembled nanoparticles,[25,48,49] including films and coatings[50] and drug delivery.[51] However, the paucity of all-acrylic PISA formulations in the literature could in part be related to the difficulty of investigating the copolymer morphology for such soft, film-forming copolymers. Furthermore, acrylic polymerizations have a well-documented propensity to undergo branching via chain transfer to polymer (CTP).[97,98] This side reaction is mitigated by the use of CRP, but not eradicated;[99] thus, a significant broadening of the molecular weight distribution is often observed.[99] There are a handful of acrylic macromolecular chain transfer agents (macro-CTAs), such as poly(acrylic acid) (PAA)[43,100] or PAA-*co*-PPEGA (poly(poly(ethylene oxide) methyl ether acrylate))[101,102] as steric stabilizers for the RAFT aqueous emulsion polymerization of styrene. Similarly, PAA has been employed as a stabilizer for the emulsion polymerization of 4-vinylpyridine (4VP) using NMP.[103] These formulations afforded a range of copolymer morphologies, but low dispersities could not be achieved at high monomer conversions.

In contrast, RAFT formulations utilizing poly(methacrylic) acid (PMAA),[104] PAA,[105,106] poly(*N,N*-dimethylacrylamide) (PDMAAm),[107,108] or poly(ethylene oxide) (PEO)[109,110] steric stabilizers in conjunction with acrylic core-forming blocks such as poly(*n*-butyl acrylate) have invariably produced kinetically trapped spheres. Moreover, cryo-TEM was required for particle imaging[105] because of the low T_g of the PBA core. Block copolymer dispersities were typically greater than 1.40, with significantly higher M_w/M_n values generally being reported at high monomer conversions.

An et al. utilized RAFT aqueous dispersion polymerization to prepare cross-linked nanogels. More specifically, either a PDMAAm[111] or poly(poly(ethylene glycol) methyl ether methacrylate) (PPEGMA)[112] stabilizer was combined with a 2-methoxyethyl acrylate-based core-forming block. This work is particularly noteworthy because relatively low dispersities were consistently obtained using a potassium persulfate/sodium ascorbate redox initiator at relatively low polymerization temperatures (30 or 40 °C). However, only spherical morphologies were reported for such formulations.

Pan and co-workers prepared poly(acrylic acid)-*b*-polystyrene (PAA−PS) diblock copolymers in the form of spheres, worms or vesicles via RAFT dispersion polymerization in methanol. However, such polymerizations were relatively slow, with significant amounts of unreacted styrene monomer still present in the formulation (conversions varied between 15 and 79%).[113] D'Agosto and co-workers[114] chain-extended a poly(*N*-acryloyl-morpholine) macro-CTA with *n*-butyl acrylate in ethanol/water mixtures using RAFT, while Charleux et al. reported the preparation of highly anisotropic worms using an all-acrylic formulation.[115] However, this required the synthesis of a bespoke cholesteryl-based monomer for the core-forming block and dispersities were relatively high (M_w/M_n = 1.3−2.0).

To date, very little work has focused on PISA using acrylic monomers in non-polar solvents. Charbonnier and co-workers utilized several monomers (4VP, and a mixture of MMA with MAA, AA or styrene) to form core-forming blocks for dispersion polymerizations in octane or toluene using NMP,[116] where either PLA or poly(2-ethylhexyl acrylate) (PEHA) was employed as the steric stabilizer. A range of spherical particles were obtained with the aim of producing electrophoretic ink but copolymer dispersities were often relatively high. There appears to be only one literature example of an all-acrylic RAFT PISA dispersion formulation in non-polar media. The Charleux group[117,118] used a poly(2-ethylhexyl methacrylate) macro-CTA to polymerize methyl acrylate in isododecane. However, only spherical particles could be obtained, while control over the copolymer molecular weight distribution was rather poor (e.g., M_w/M_n = 1.76 at 48% conversion).[118]

Herein an all-acrylic RAFT dispersion polymerization formulation is examined for the preparation of poly(lauryl acrylate)−poly(benzyl acrylate) (PLA−PBzA) nanoparticles in *n*-heptane, *n*-dodecane or isohexadecane. The copolymer morphology could be adjusted by varying the target degree of polymerization (DP) of the PBzA block, the copolymer concentration, and the solvent type. A phase diagram was constructed for the *n*-heptane formulation based on the visual appearance of the samples, dynamic light scattering (DLS) data, and our prior experience of related methacrylic PISA formulations. Selected copolymers were also characterized by cryo-TEM, which confirmed our morphology assignments. In particular, a soft, free-standing gel phase was identified that proved to be thermoresponsive. Finally, these all-acrylic copolymer dispersions can be conveniently prepared via a one-pot protocol at 40% w/w solids.

■ EXPERIMENTAL SECTION

Materials. Lauryl acrylate (LA, 98%) was purchased from Tokyo Chemical Industry UK Ltd., and benzyl acrylate (BzA, 97%) was purchased from Alfa Aesar; both were used as received. 2,2′-Azoisobutyronitrile (AIBN, 98%), 2-(dodecylthiocarbonothioylthio)-2-methylpropanoic acid (DDMAT, 98%) and deuterated chloroform (CDCl$_3$) were purchased from Sigma-Aldrich (UK) and were used as

received. *tert*-Butylperoxy-2-ethylhexanoate (Trigonox 21S or T21s) initiator was supplied by AkzoNobel (The Netherlands). All other reagents were purchased from Sigma-Aldrich (UK) and were used as received, unless otherwise noted. *n*-Heptane ($\geq$96%) and *n*-dodecane ($\geq$99%) were purchased from Fisher Scientific (UK). Isohexadecane (main constituent of a 97% w/w mix of C_{16} isoparaffins) was donated by Scott Bader (Wollaston, UK) and used without further purification. All other solvents were of HPLC quality and were purchased from Fisher Scientific (Loughborough, UK).

Synthesis of PLA_x Macro-CTA. A typical protocol for the synthesis of a PLA_{14} macro-CTA was as follows. LA monomer (0.32 mol, 76.922 g), DDMAT RAFT agent (12.8 mmol, 4.667 g), and acetone (1.41 mol, 82.009 g) were added to a round-bottomed flask in order to target a mean degree of polymerization (DP) of 25. AIBN initiator (2.56 mmol, 0.420 g, CTA/AIBN molar ratio = 5.0) was added to this mixture, and the resulting yellow solution was cooled in an ice bath while sparging with N_2 gas for 30 min, before the sealed flask was immersed in an oil bath set at 70 °C. After 125 min, the polymerization was quenched by immersion of the reaction flask in ice, followed by exposure to air (55% LA conversion, determined by ^{1}H NMR spectroscopy). The crude polymer solution was then precipitated twice into a 10-fold excess of cold methanol and washed in this non-solvent before being dried under high vacuum for 3 days at 20 °C. ^{1}H NMR analysis indicated a mean DP of 14 for this PLA macro-CTA. This suggests a CTA efficiency of 98%. THF GPC analysis indicated M_n and M_w/M_n values of 3 700 g mol^{-1} and 1.12, respectively.

Synthesis of PLA_{14}–$PBzA_y$ Diblock Copolymers via RAFT Dispersion Polymerization. A typical protocol for the synthesis of PLA_{14}–$PBzA_{90}$ diblock copolymer was as follows: PLA_{14} macro-CTA (0.165 g, 0.04 mmol) was added to a 25 mL round-bottomed flask (or a glass vial), followed by BzA monomer (0.6457 g, 3.98 mmol) and *n*-heptane (3.0595 g). T21S initiator was then added (1.9 mg, 0.009 mmol), as a 1.0% solution in *n*-heptane to make up a 20% w/w solution (CTA/T21S molar ratio = 5.0). This flask was cooled using an ice bath, and the solution was sparged with N_2 gas for 25 min. The flask was then sealed and immersed in an oil bath set at 80 °C. The reaction mixture was stirred for 16 h to ensure high monomer conversion (98% by ^{1}H NMR analysis) and subsequently quenched by cooling followed by exposure to air. THF GPC analysis indicated M_n and M_w/M_n values of 14 000 g mol^{-1} and 1.89, respectively.

One-Pot Synthesis of PLA_{15}–$PBzA_y$ Diblock Copolymer Nanoparticles via RAFT Dispersion Polymerization. LA monomer (0.01 mol, 2.4038 g) was added to a round-bottomed flask containing DDMAT RAFT agent (0.66 mmol, 0.2430 g) in order to target a mean degree of polymerization (DP) of 15. AIBN initiator (0.13 mmol, 0.0219 g, CTA/AIBN molar ratio = 5.0) was then added to this flask, and the resulting yellow solution was cooled in ice prior to N_2 sparging for 30 min, before the sealed flask was immersed into an oil bath set at 70 °C. After 105 min (97% conversion, determined by ^{1}H NMR), the polymerization was quenched by immersing the flask in an ice bath followed by exposure to air. A small amount of the crude PLA macro-CTA was then precipitated twice into a 10-fold excess of cold methanol and washed in this non-solvent before being dried under high vacuum for 3 days at 20 °C. ^{1}H NMR analysis indicated a DP of 15 for this PLA macro-CTA, which suggests a CTA efficiency of 97%. THF GPC analysis indicated M_n and M_w/M_n values of 4 300 g mol^{-1} and 1.10, respectively. The remaining crude PLA_{15} macro-CTA (0.190 g, 0.047 mmol) was added to a 25 mL round-bottomed flask, followed by addition of BzA monomer (0.6209 g, 3.82 mmol, target DP = 80) and *n*-heptane (3.0453 g). T21S was then added (2.1 mg, 0.0096 mmol; CTA/T21S molar ratio = 5.0) in the form of a 1.0% solution in *n*-heptane (0.21 mL) to make up a 20% w/w solution, and the solution was cooled using an ice bath and sparged with N_2 for 25 min. The flask was sealed and immersed in an oil bath set at 80 °C. The reaction solution was then stirred for 16 h to ensure high monomer conversion (99% by ^{1}H NMR analysis) and subsequently quenched by cooling to 20 °C followed by exposure to air. THF GPC analysis indicated M_n and M_w/M_n values of 13 800 g mol^{-1} and 1.97, respectively.

Copolymer Characterization. *^{1}H NMR Spectroscopy.* All NMR spectra were recorded using a 400 MHz Bruker Avance-400 spectrometer (64 scans per sample) in CDCl$_3$.

Gel Permeation Chromatography (GPC). Molecular weight distributions were assessed by GPC using a THF eluent. The GPC setup consisted of two 5 μm (30 cm) "Mixed C" columns as part of a Polymer Laboratories PL-GPC-50 unit and used a WellChrom K-2301 refractive index detector operating at 950 ± 30 nm. The mobile phase contained 2.0% v/v triethylamine and 0.05% w/v butylhydroxytoluene (BHT), and its flow rate was fixed at 1.0 mL min^{-1}. A series of ten near-monodisperse poly(methyl methacrylate) standards (M_p values ranging from 1 280 to 330 000 g mol^{-1}) were used for calibration. Chromatograms were analyzed using Cirrus GPC software provided by the manufacturer.

Dynamic Light Scattering (DLS). Intensity-average hydrodynamic diameters for the dispersions were obtained by DLS using a Malvern Zetasizer Nano ZS instrument. *n*-Heptane, *n*-dodecane, or isohexadecane dispersions of 0.20% w/w solids were analyzed using a 1 cm quartz cuvette, and all data were averaged over three consecutive runs.

Transmission Electron Microscopy (TEM). Diblock copolymer dispersions were diluted at 20 °C to generate 0.20% w/w dispersions. Copper TEM grids (Agar Scientific, UK) were surface-coated in-house to yield a thin film of amorphous carbon. Each diblock copolymer dispersion (0.20% w/w, 11 μL) was placed onto a grid for 1 min and then blotted with filter paper to remove excess solution. To stain the deposited nanoparticles, the grids were exposed to ruthenium(IV) oxide vapor for 7 min at 20 °C prior to analysis.[91] This heavy metal compound acted as a positive stain to improve contrast. The ruthenium(IV) oxide was prepared as follows: ruthenium(II) oxide (0.30 g) was added to water (50 g) to form a black slurry; addition of sodium periodate (2.0 g) with stirring produced a yellow solution of ruthenium(IV) oxide within 1 min. Imaging was performed at 100 kV using a Phillips CM100 instrument equipped with a Gatan 1k CCD camera.

Cryogenic Transmission Electron Microscopy (Cryo-TEM). Sample vitrification was conducted using an automated vitrification robot (FEI VitrobotTM Mark III) for the liquid nitrogen quench. Cryo-TEM 200 mesh copper grids with a "lacey" carbon film (EM Resolutions, UK) were used without plasma treatment. For vitrification, typically 3 μL of dispersion (<1.0% w/w in *n*-heptane) was applied to a cryo-TEM grid inside the vitrobot chamber at 20 °C. Samples were examined using a FEI Tecnai Spirit TEM instrument equipped with a Gatan 1k MS600CW CCD camera operating at 120 kV under low-dose conditions. Vitrified grids were mounted onto a cryo-transfer holder precooled to −175 °C using liquid nitrogen and then transferred into the microscope. The *n*-heptane solvent film was not vitreous at −175 °C but appeared to be thick and crystalline, which prevented imaging of the copolymer nano-objects. Therefore, the *n*-heptane was freeze-dried inside the microscope by warming the holder using a Gatan Model 900 SmartSet temperature controller. For worm and vesicle dispersions, the holder was warmed to −95 °C and maintained at this temperature while micrographs were recorded. Under these conditions, the frozen *n*-heptane was removed under vacuum inside the microscope to reveal the embedded nano-objects clinging to the edges of the supporting "lacey" carbon membrane (vesicles) or spanning the holes in the film (worms). For spherical nanoparticle dispersions, the holder was warmed to −110 °C and maintained at this temperature for imaging. Under these conditions, most of the *n*-heptane was removed by the vacuum, but the remaining frozen solvent was both amorphous and sufficiently thin to reveal the embedded spheres for imaging. Micrographs were recorded at magnifications ranging from 18 500 to 98 000, with defocus values of between −40 and −5 μm.

Rheology Measurements. An AR-G2 rheometer equipped with a variable temperature Peltier plate and a 40 mm 2° aluminum cone was used for all experiments. Viscosity, loss modulus, and storage modulus were measured as a function of percentage strain, angular frequency, and temperature to assess the critical gelation temperature, gel stiffness, and gel viscosity of selected worm gels. Percentage strain sweeps were conducted between 4 and 80 °C using a constant angular frequency of 10 rad s^{-1}. Angular frequency sweeps were conducted at various temperatures using a fixed strain of 1.0%. Temperature sweeps were also
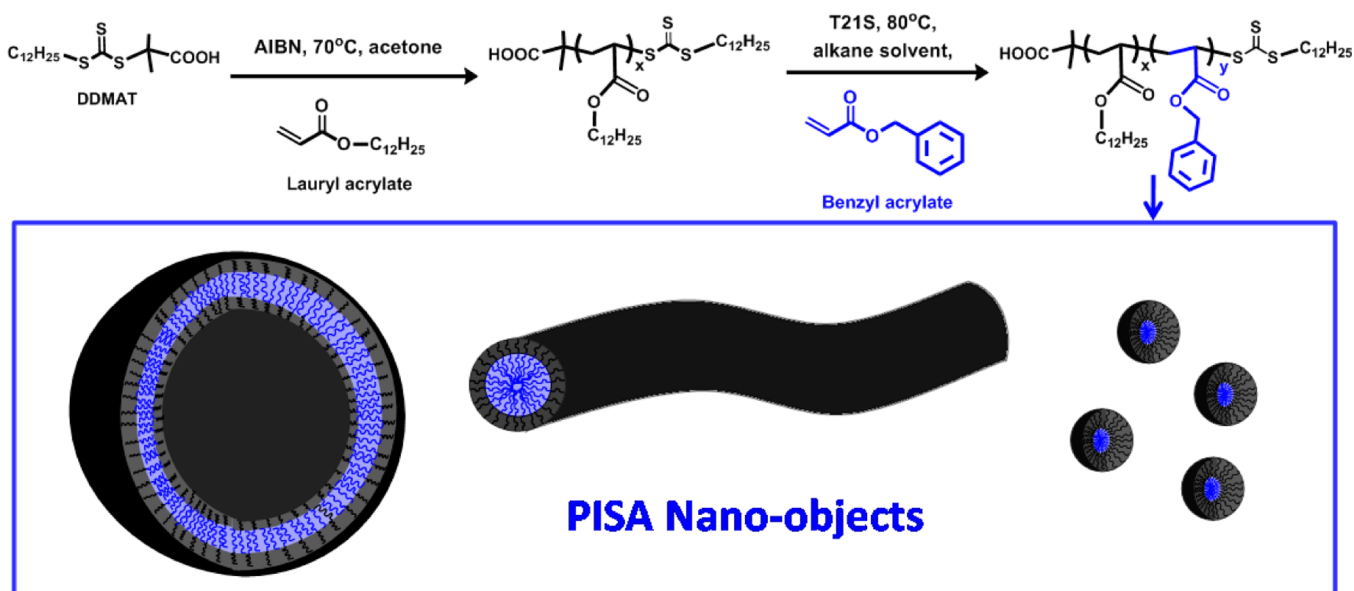
Figure 1. Schematic representation of the synthesis of PLA_{14}-$PBzAy$ copolymers prepared via RAFT dispersion polymerization in non-polar media (*n*-heptane, *n*-dodecane, or isohexadecane) at 80 °C. As the target DP of the PBzA core is increased, the copolymers spontaneously self-assemble to produce spherical, worm-like, or vesicular nano-objects.
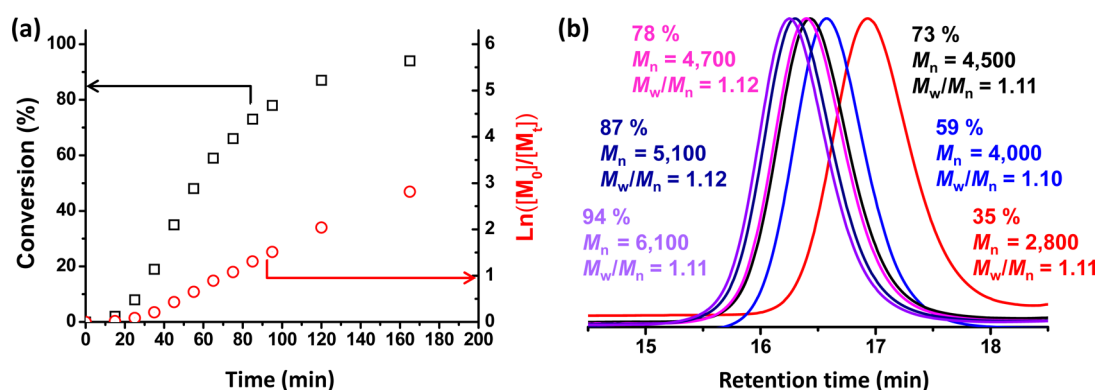
Figure 2. (a) Conversion vs time curve for the synthesis of a PLA macro-CTA (target DP = 25) in an oil bath set at 70 °C using a CTA/T21S molar ratio of 5.0 at 50% w/w solids in acetone. The reaction mixture was sampled at various time intervals, and conversions were assessed using ^{1}H NMR analysis. First-order kinetics were observed after a relatively short induction period of approximately 20 min. (b) Selected THF GPC traces obtained for the same PLA macro-CTA synthesis with corresponding monomer conversions, molecular weights, and M_w/M_n values.

conducted at 1.0% strain using an angular frequency of 10 rad s^{-1}. In these latter experiments, the temperature was varied by 2 °C between each measurement, allowing an equilibration time of 2 min in each case.

RESULTS AND DISCUSSION

Homopolymerization of LA. In 2013, Fielding et al. published an example of an *all-methacrylic* RAFT PISA formulation based on a PLMA−PBzMA diblock copolymer formulation in *n*-heptane.[91] They were able to prepare a range of well-defined nano-objects, including a pure worm phase that formed relatively transparent free-standing gels. In the present work, an analogous all-acrylic formulation has been developed via chain extension of a PLA macro-CTA using benzyl acrylate (BzA) in a range of non-polar solvents.

The RAFT solution polymerization of LA (target DP = 25) was conducted in acetone at 70 °C using an AIBN initiator (see Figure 1). DDMAT was selected for this synthesis as trithiocarbonates are known to efficiently control the polymerization of acrylic monomers.[119] A conversion of 94% was obtained after ∼3 h, determined by ^{1}H NMR (see Figure 2a,b),

and the linear semilogarithmic plot indicated first-order kinetics with respect to LA. The THF GPC data shown in Figure 2b confirm the unimodal nature of the PLA molecular weight distribution over the course of the reaction. The molecular weight increases linearly with conversion and low dispersities (below 1.12) are observed throughout. Subsequently, a large batch of PLA (target DP = 25) was prepared and the polymerization quenched after 65 min (55% conversion, determined by ^{1}H NMR). The crude PLA was then precipitated twice into a 10-fold excess of cold methanol and washed in this non-solvent, before being placed under high vacuum for 3 days at 20 °C. ^{1}H NMR analysis indicated a mean DP of 14 for this PLA macro-CTA, which corresponds to a relatively high CTA efficiency of 98%. This was calculated by comparing the DP of the polymer after purification by precipitation with the monomer conversion. In both cases this was calculated from the molar ratio of DDMAT to PLA protons (labeled "d' and 'h", respectively; see Figure 3a).

Dispersion Polymerization of BzA in *n*-Heptane. The synthesis conditions for a PLA_{14}−BzA_{140} diblock copolymer
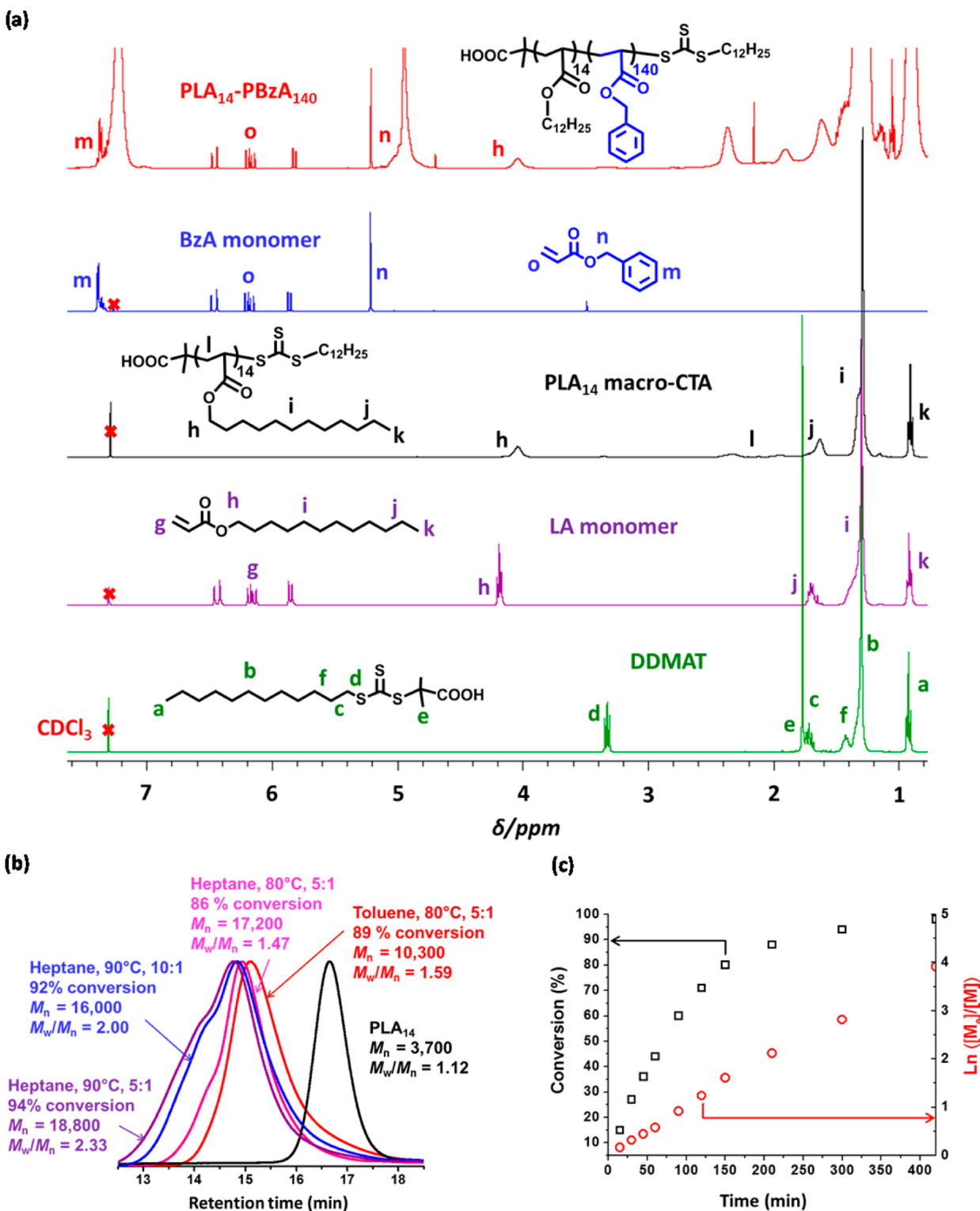
Figure 3. (a) ^{1}H NMR spectra (CDCl$_3$) recorded for PLA$_{14}$−PBzA$_{140}$ diblock copolymer (94% BzA conversion, polymerized in *n*-heptane, 90 °C, CTA/T21S 5:1), BzA monomer, PLA$_{14}$ macro-CTA, lauryl acrylate (LA) monomer, and the DDMAT CTA. (b) Series of THF GPC traces obtained for PLA$_{14}$−PBzA$_{140}$ diblock copolymers synthesized at 20% w/w under various conditions (polymerization solvent, temperature, and CTA/T21S molar ratio are shown in parentheses). The monomer conversions (determined by ^{1}H NMR analysis after sampling at 7 h) and molecular weight data are displayed for each trace. (c) Conversion vs time curves obtained for the BzA polymerization when targeting a PLA$_{14}$−PBzA$_{100}$ diblock copolymer at 80 °C using a CTA/T21S molar ratio of 5.0 at 20% w/w solids in *n*-heptane. This polymerization exhibits first-order kinetics with respect to BzA monomer.

were systematically varied to identify the ideal conditions required for a well-controlled RAFT polymerization. A series of THF GPC curves for PLA$_{14}$−PBzA$_{140}$ diblock copolymers are shown in Figure 3b. The RAFT *solution* polymerization of BzA in

toluene (which is a good solvent for both blocks) results in a slightly higher M_w/M_n value than the equivalent dispersion polymerization in *n*-heptane (both conducted at 20% w/w total solids, 80 °C, macro-CTA/initiator = 5.0). This might be due to a

Table 1. Summary of Synthesis Conditions, Final Monomer Conversions, and GPC Data Obtained for a Series of PLA$_{14}$−PBzA$_y$ Copolymers Prepared via RAFT Dispersion Polymerization of BzA in *n*-Heptane[a]

entry no.	targeted diblock composition	solids content (% w/w)	conversion (%)	M_n (g mol^{-1})	M_w/M_n	visual appearance
1	PLA$_{14}$−PBzA$_{70}$	30	99	11 800	1.58	transparent gel
2	PLA$_{14}$−PBzA$_{55}$	25	99	10 600	1.55	slightly turbid liquid
3	PLA$_{14}$−PBzA$_{60}$	25	99	10 200	1.53	slightly turbid gel
4	PLA$_{14}$−PBzA$_{70}$	25	99	11 800	1.59	slightly turbid gel
5	PLA$_{14}$−PBzA$_{80}$	25	99	12 900	1.63	milky gel
6	PLA$_{14}$−PBzA$_{90}$	25	99	13 600	1.67	milky liquid
7	PLA$_{14}$−PBzA$_{45}$	20	99	9 400	1.47	slightly turbid liquid
9	PLA$_{14}$−PBzA$_{55}$	20	98	10 500	1.36	slightly turbid liquid
10	PLA$_{14}$−PBzA$_{60}$	20	99	11 300	1.56	slightly turbid liquid
11	PLA$_{14}$−PBzA$_{70}$	20	99	11 600	1.76	slightly turbid gel
12	PLA$_{14}$−PBzA$_{80}$	20	99	12 200	1.81	milky gel
13	PLA$_{14}$−PBzA$_{90}$	20	98	14 000	1.89	milky liquid
14	PLA$_{14}$−PBzA$_{100}$	20	99	17 500	1.81	milky liquid[b]
15	PLA$_{14}$−PBzA$_{60}$	15	97	11 200	1.52	slightly turbid liquid
16	PLA$_{14}$−PBzA$_{65}$	15	98	11 700	1.65	slightly turbid liquid
17	PLA$_{14}$−PBzA$_{70}$	15	97	13 700	1.99	slightly turbid gel
18	PLA$_{14}$−PBzA$_{80}$	15	97	12 800	1.69	milky gel
19	PLA$_{14}$−PBzA$_{90}$	15	97	15 400	1.82	milky liquid
20	PLA$_{14}$−PBzA$_{70}$	10	90	12 300	1.62	slightly turbid liquid
21	PLA$_{14}$−PBzA$_{80}$	10	90	12 300	1.71	slightly turbid gel
22	PLA$_{14}$−PBzA$_{90}$	10	92	14 000	2.10	turbid liquid
23	PLA$_{14}$−PBzA$_{80}$	7.5	88	13 000	1.84	turbid liquid
24	PLA$_{14}$−PBzA$_{90}$	7.5	90	14 000	2.05	turbid liquid[b]
25	PLA$_{14}$−PBzA$_{105}$	7.5	86	15 200	2.05	turbid liquid[b]
26	PLA$_{14}$−PBzA$_{90}$	5	75	17 700	1.92	turbid liquid
27	PLA$_{14}$−PBzA$_{150}$	5	63			phase separation[b]

[a]All polymerizations were conducted using a CTA/T21S molar ratio of 5.0 at 80 °C. Conversions were assessed using ^{1}H NMR spectroscopy, and molecular weight data were obtained via THF GPC (using a series of near-monodisperse poly(methyl methacrylate) calibration standards). [b]Partial sedimentation was observed after the initial dispersion was allowed to stand at 20 °C for several days.

slightly less efficient chain extension in toluene, since there appears to be a larger proportion of unreacted macro-CTA in the THF GPC trace.

The chain extension in *n*-heptane appears to be more efficient resulting in a lower dispersity (under the equivalent conditions of 80 °C and CTA/T21S molar ratio = 5.0). However, in general, the M_w/M_n values indicated in Figure 3b are significantly higher than expected for a well-controlled RAFT polymerization. Unfortunately, this is not uncommon for all-acrylic formulations[105,117,118] and could well be due to the aforementioned and well-documented chain transfer to the polymer backbone,[97,98] which inevitably leads to extensive branching.[99] Indeed, other all-acrylic formulations such as the dispersion polymerization described by Charleux and co-workers[115] in alcohol/water mixtures also suffer from higher than expected copolymer dispersities. When DPs greater than 40 were targeted, M_w/M_n values above 1.9 were observed. Moreover, this loss of control was more pronounced when higher monomer conversions were obtained. Similar observations were also reported for an alkane-based dispersion polymerization formulation reported by the same group.[118] However, in this case substantially higher dispersities were observed: monomer conversions above 62% resulted in M_w/M_n values above 4.0. Nonetheless, in the present case high monomer conversions were still obtained in most cases as determined by ^{1}H NMR (>97% at 15% w/w solids and above), with M_w/M_n < 2.0 in most cases (see Table 1). Monomer conversions were calculated by comparing the integrated vinyl signals in Figure 3a (labeled "o" in the case of BzA and "g" for LA monomer) to that of the polymer signals (signal "n" in the case of

PBzA and "h" for PLA). ^{1}H NMR spectra recorded for the respective monomers and the CTA used in this formulation are also shown, along with a representative example of the diblock copolymer. Attempts to increase the rate of polymerization by performing syntheses at 90 °C were successful but resulted in a large increase in M_w/M_n even at higher macro-CTA/initiator molar ratios. Conducting the polymerizations at 70 °C did not lead to narrower molecular weight distributions but resulted in significantly slower rates of polymerization (data not shown), so it was decided to conduct all further PLA$_{14}$−PBzA$_y$ syntheses at 80 °C using a macro-CTA/T21S molar ratio of 5.0. The kinetics of polymerization of BzA when targeting PLA$_{14}$−PBzA$_{100}$ was subsequently studied under such conditions using ^{1}H NMR spectroscopy. Regular sampling of the polymerization (see Figure 3c) resulted in a linear semilogarithmic plot, indicating first-order kinetics with respect to monomer.[120] Although 90% conversion was achieved after just 4 h, the rate of polymerization became significantly slower after this point, with only 98% conversion being achieved after 7 h. Thus, unless otherwise stated, polymerizations were typically run for 16 h to ensure high monomer conversions. Digital photographs recorded for PLA$_{14}$−PBzA$_{100}$ diblock copolymer dispersions at various time points (see Figure 4) clearly show an increase in turbidity between 30 min and 1.5 h. Perhaps more interestingly, a change in the rheological behavior of the dispersion was observed at 1.5 h, as the weakly turbid free-flowing fluid became a weakly turbid free-standing gel. After 2.5 h, the gel became a turbid/milky free-flowing fluid. Diluting these dispersions to 0.20% w/w solids
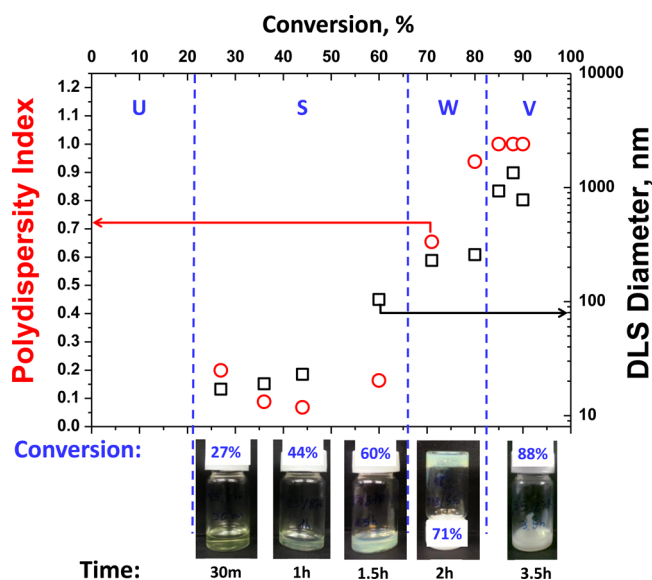
Figure 4. Intensity-average diameter and DLS polydispersity index for 0.20% w/w PLA$_{14}$−PBzA$_{100}$ copolymer dispersions in *n*-heptane at 20 °C, sampled at different time points. The corresponding BzA conversions and digital images (taken at 20 °C) of the original concentrated dispersion are also shown. PLA$_{14}$−PBzA$_{100}$ diblock copolymer was synthesized at 80 °C using a CTA/T21S molar ratio of 5.0 at 20% w/w solids in *n*-heptane. Nucleation occurs at a BzA conversion of between 15% (U = unimers) and 27% (S = spheres), with the particles undergoing subsequent morphological transitions to produce worms (W) at around 60% conversion and vesicles (V) above 80% conversion. These order−order transitions result in a significant increase in DLS polydispersity index from 0.07 to 1.0. However, it is important to note that DLS only reports a sphere-equivalent hydrodynamic particle diameter. Thus, for highly anisotropic particles such as worms, this technique only provides a rather crude estimate of the particle size.

allowed particle size analysis by dynamic light scattering (DLS) (see Figure 4).

DLS studies indicate an increase in the apparent sphere-equivalent hydrodynamic particle diameter with conversion, which is consistent with the observed increase in turbidity. A discernible increase in turbidity after 30 min suggested the onset of particle nucleation, with DLS indicating an intensity-average diameter of 17 nm at this time point. The mean particle diameter gradually increased up to 23 nm after 1 h. An abrupt increase in size to 104 nm occurred after 1.5 h, which was accompanied by a significant increase in turbidity. Initially, relatively narrow particle size distributions were obtained (DLS polydispersities (PDI) 0.07−0.19). However, much broader size distributions were observed after 1.5 h (PDI > 0.60). In this context, it is worth noting that similar changes in DLS particle diameter/polydispersity and physical appearance were reported by Fielding et al.[91] for the analogous all-methacrylic PLMA−PBzMA PISA syntheses. Of course, this does not provide conclusive evidence for similar morphologies in the case of these PLA−PBzA dispersions. Nevertheless, we hypothesized that the slightly turbid dispersions observed for relatively short PBzA DPs corresponded to spherical micelles, the gel phase formed at longer PBzA DPs indicated the presence of anisotropic worms, and the relatively turbid (milky) dispersions formed when targeting the longest PBzA DPs most likely corresponded to vesicle formation. Thus, the physical appearance of the

dispersions combined with our DLS observations was used to make an initial assessment of the copolymer morphology.

The effect of systematically varying the target DP of the core-forming PBzA block and copolymer concentration for a series of PLA$_{14}$−PBzA$_x$ copolymers prepared via PISA was subsequently investigated (see Table 1).

Lower dispersities and higher blocking efficiencies (see Figure 5) and higher conversions (see Table 1) are generally observed
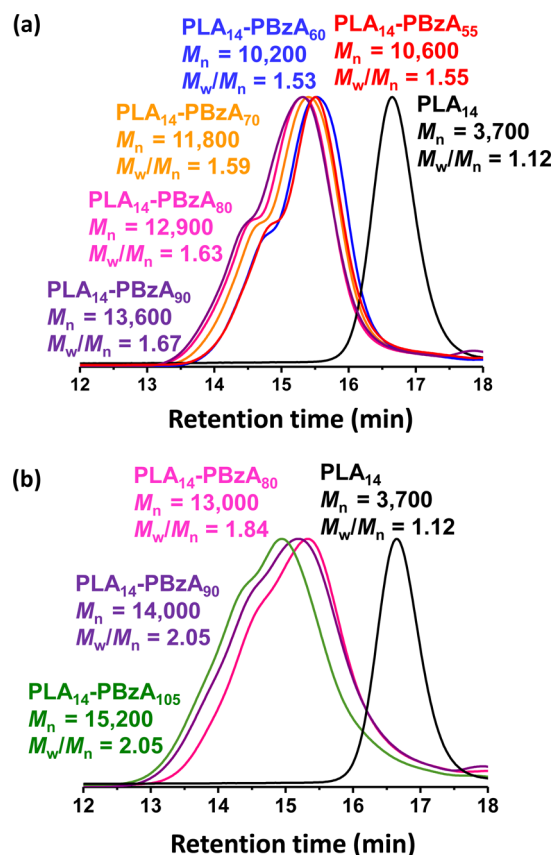
Figure 5. THF GPC traces obtained for (a) PLA$_{14}$−PBzA$_y$ diblock copolymers synthesized at 25% w/w solids and (b) PLA$_{14}$−PBzA$_y$ diblock copolymers synthesized at 7.5% w/w solids in *n*-heptane at 80 °C using a CTA/T21S molar ratio of 5.0. PISA syntheses conducted at 7.5% w/w solids led to incomplete conversions, whereas those conducted at 25% w/w solids attained more than 99% conversion (see Table 1).

for polymerizations conducted at higher copolymer concentrations. For example, a PLA$_{14}$−PBzA$_{80}$ copolymer prepared at 7.5% w/w solids attained 88% conversion and exhibited a final M_w/M_n of 1.84. However, targeting the same copolymer at 15% w/w solids led to a conversion of 97% and an M_w/M_n of 1.69, whereas at 25% w/w solids the corresponding values were 99% and 1.63, respectively (compare entries 5, 18, and 23 in Table 1). This suggests a gradual loss of RAFT control at lower copolymer concentrations, in addition to the problem of chain transfer to polymer discussed previously. For example, Veloso et al.[121] recently undertook a detailed study of the RAFT solution polymerization of *n*-butyl acrylate using a trithiocarbonate-based chain transfer agent in various solvents (e.g., ethanol, toluene, etc.). Their findings suggested that the predominant cause of dead chains in this RAFT formulation originated from chain transfer to solvent. Clearly, this side reaction is likely to become more prevalent at lower copolymer concentrations (since there is
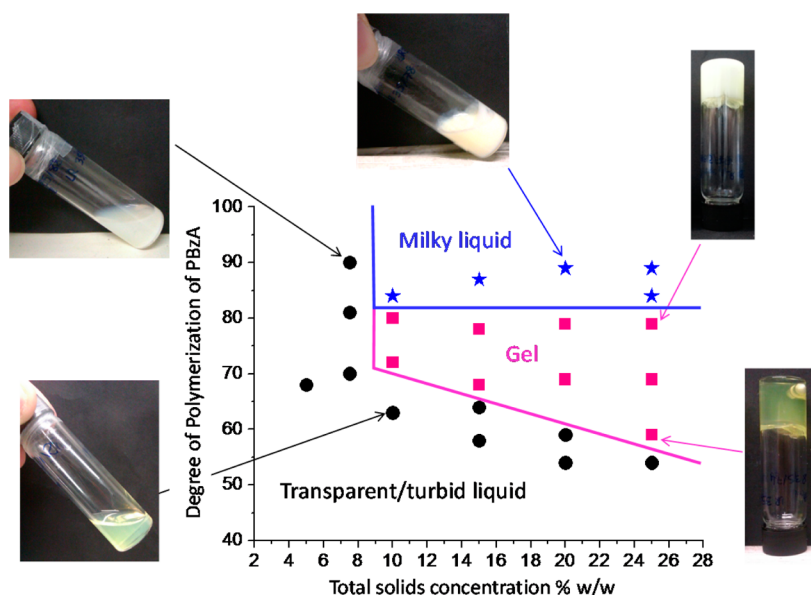
Figure 6. Phase diagram constructed for PLA$_{14}$-PBzA$_y$ diblock copolymers prepared at 80 °C by RAFT dispersion polymerization in *n*-heptane. The degree of polymerization (DP) of the core-forming block is the actual DP of PBzA, calculated from the final conversion of each polymerization, determined by ^{1}H NMR spectroscopy. Digital photographs (taken at 20 °C) indicate the physical appearance of selected diblock copolymer dispersions, which was used to assign the phase boundaries. Free-flowing transparent (or relatively low turbidity) dispersions contain mainly spheres, gels contain predominantly worms, and highly turbid free-flowing dispersions were assigned as vesicles. These preliminary assignments were consistent with subsequent DLS measurements (see Table 1) and also selected cryo-TEM studies (see Figure 7).

necessarily a higher proportion of solvent). Dispersion polymerization conditions and *n*-alkane-based solvents were not examined by Veloso et al., but it seems likely that chain transfer to solvent would also occur in this case. However, confirming this hypothesis would require further experimental studies, which are beyond the scope of the present study. Of course, the high molecular weight shoulder that is observed in the GPC traces could also be attributed to some degree of termination by combination, which is the dominant mechanism for acrylic polymers.

At a copolymer concentration of 10% w/w solids or higher, two different types of dispersion are observed. Increasing the DP of the PBzA block results in the transformation from a weakly turbid, free-flowing liquid to a free-standing gel, which increases in turbidity until finally a milky-white free-flowing liquid is observed. Polymerizations conducted at more than 10% w/w solids also produced dispersions that were very similar in physical appearance to the copolymers obtained by the *in situ* sampling method described in Figure 4. A detailed phase diagram was constructed (see Figure 6), with high conversions being obtained after 16 h at 80 °C for each synthesis (see Table 1). The inset digital photographs indicate the final visual appearance of selected copolymer dispersions at 20 °C. DLS studies indicated that only relatively small particles were obtained at or below 8% w/w solids, which is consistent with the low turbidities and free-flowing nature of these dispersions. Similar observations were also made for dispersions prepared at higher copolymer concentrations when targeting shorter PBzA DPs.

The milky-white free-flowing dispersions tended to become colloidally unstable for PBzA DPs > 90 (increasing amounts of sedimentation were observed at all copolymer concentrations). Perhaps above this DP the PLA macro-CTA is no longer an efficient enough stabilizer for the PBzA core, resulting in the very large or aggregated particles observed by DLS measurements (see data in Figure S1 in the Supporting Information). The gel phase region is initially almost transparent, with only weak

turbidity being observed at lower PBzA DPs, which gradually becomes milky white at the DP increases.

Characterization of Copolymer Morphology. Initially, conventional TEM was used to examine copolymer morphologies, as described by Fielding et al.[91] PLA$_{14}$−PBzA$_y$ diblock copolymers (where y = 60, 70, 80, or 90) prepared at 20% w/w solids in *n*-heptane were examined, since these dispersions represented the main classes of dispersion: free-flowing turbid liquid, gel (slightly turbid and milky), and milky liquid. However, despite examining various staining/deposition methods, only rather poorly defined agglomerated particles could be observed whose dimensions did not correspond to those indicated by DLS studies (see Figure S1). Similar problems were encountered for particles prepared in *n*-dodecane (DD) or isohexadecane (IHD) (data not shown). This is attributed to the relatively low T_g of the PBzA core (literature value = 6 °C),[122] which results in partial particle coalescence during TEM grid preparation.

Two strategies were examined to overcome this problem. First, particles were cross-linked by introducing ethylene glycol diacrylate (EGDA) as a third comonomer. In principle, intraparticle cross-linking should make the particles more robust, ideally without perturbing their copolymer morphology. Hence, EGDA was added to each dispersion at 80 °C after conducting the BzA polymerization for 7 h. ^{1}H NMR analysis indicated at least 98% conversion of BzA monomer at this point in all cases. DLS studies were conducted both before EGDA addition (in *n*-dodecane) and after EGDA addition (in THF). The latter solvent is a good solvent for the PBzA core-forming block, so a comparable particle size is only expected under these conditions if cross-linking had been successful. Moreover, ^{1}H NMR spectra recorded for cross-linked particles dispersed in CDCl$_3$ indicated attenuated PBzA signals and confirmed EGDA conversions of more than 85% in all cases. TEM images recorded for the cross-linked particles prepared in *n*-dodecane were much more encouraging than those obtained for the corresponding linear diblock copolymer nanoparticles (compare Figures S1 and S2).
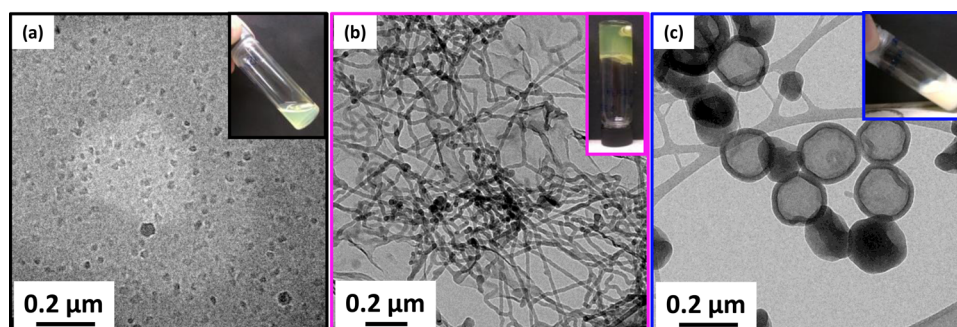
Figure 7. Selected cryo-TEM images obtained for (a) 0.75% w/w dispersion of PLA$_{14}$−PBzA$_{65}$ copolymer prepared at 15% w/w solids in *n*-heptane, (b) 0.20% w/w dispersion of PLA$_{14}$−PBzA$_{70}$ copolymer prepared at 20% w/w solids in *n*-heptane, and (c) 0.1% w/w PLA$_{14}$−PBzA$_{95}$ copolymer synthesized at 20% w/w solids in *n*-heptane. In each case dispersions were diluted with *n*-heptane at 20 °C. Digital photographs of the physical appearance of the as-synthesized concentrated dispersions are also shown.

Table 2. Summary of Synthesis Conditions, Final Monomer Conversions, and GPC Data Obtained for a Series of PLA$_{14}$−PBzA$_{y}$ Copolymers Prepared via RAFT Dispersion Polymerization of BzA Conducted in Either *n*-Dodecane (DD) or Isohexadecane (IHD)[a]

entry no.	target composition	solids (% w/w)	solvent type	conversion (%)	M_n (g mol^{-1})	M_w/M_n	visual appearance
1	PLA$_{14}$−PBzA$_{60}$	40	DD	99	11 000	1.44	transparent gel
2	PLA$_{14}$−PBzA$_{40}$	20	DD	99	8 900	1.45	slightly turbid liquid
3	PLA$_{14}$−PBzA$_{50}$	20	DD	99	10 300	1.49	slightly turbid liquid
4	PLA$_{14}$−PBzA$_{60}$	20	DD	99	10 800	1.66	slightly turbid gel
5	PLA$_{14}$−PBzA$_{70}$	20	DD	99	11 500	1.74	milky gel
6	PLA$_{14}$−PBzA$_{80}$	20	DD	99	13 740	1.66	milky liquid
7	PLA$_{14}$−PBzA$_{90}$	20	DD	99	14 500	1.69	milky liquid[b]
8	PLA$_{14}$−PBzA$_{60}$	15	DD	98	11 000	1.69	slightly turbid gel
9	PLA$_{14}$−PBzA$_{70}$	15	DD	99	12 700	1.71	milky gel
10	PLA$_{14}$−PBzA$_{40}$	20	IHD	99	8 500	1.43	slightly turbid liquid
11	PLA$_{14}$−PBzA$_{50}$	20	IHD	99	9 900	1.50	slightly turbid gel
12	PLA$_{14}$−PBzA$_{60}$	20	IHD	99	11 300	1.41	milky gel
13	PLA$_{14}$−PBzA$_{70}$	20	IHD	99	12 900	1.51	milky liquid
14	PLA$_{14}$−PBzA$_{50}$	15	IHD	99	10 200	1.53	slightly turbid liquid
15	PLA$_{14}$−PBzA$_{60}$	15	IHD	99	11 100	1.44	slightly turbid gel

[a]All syntheses were conducted using a CTA/T21S molar ratio of 5.0 at 80 °C. Conversions were assessed using ^{1}H NMR spectroscopy, and molecular weight data were determined via THF GPC (using a series of near-monodisperse poly(methyl methacrylate) calibration standards). [b]Partial sedimentation was observed after several days.

Relatively small, pseudospherical particles were observed for PLA$_{14}$−PBzA$_{45}$−PEGDA$_6$, worm-like clusters were obtained for PLA$_{14}$−PBzA$_{60}$−PEGDA$_6$ (resulting in a stiffer gel; see Figure S3), and relatively large vesicular structures were formed by PLA$_{14}$−PBzA$_{90}$−PEGDA$_6$. Thus, intra-particle cross-linking can to some extent alleviate the intrinsic problems associated with TEM analysis of soft film-forming particles.

Subsequently, cryo-TEM was utilized to characterize a subset of copolymer dispersions. It is well-known that this technique enables imaging of soft particles, since they are trapped within a thin vitreous film of rapidly frozen solvent.[123] However, although cryo-TEM is widely used for imaging biological specimens and synthetic nanomaterials in *aqueous* media, there are very few literature reports describing cryo-TEM studies in *non-polar* solvents.[123−126] In the present work, liquid nitrogen was used to vitrify *n*-heptane dispersions, since this cryogen is known to have high solubility in *n*-alkanes (e.g., liquid ethane). However, the relatively slow freezing rate of liquid nitrogen led to crystallization of the *n*-heptane phase and so reduced the electron contrast of the embedded particles. Thus, *n*-heptane was sublimed inside the microscope by heating from around −175 to −95 °C in order to gradually reveal the morphology of the embedded particles. Three dispersions were imaged that

corresponded to a free-flowing dispersion of relatively low turbidity, a free-standing gel, and a highly turbid free-flowing dispersion. As anticipated, the respective predominant copolymer morphologies were confirmed to be spheres, worms, and vesicles respectively (see Figure 7). However, it is worth noting that all characterization of these diblock copolymer dispersions has been conducted at 20 °C. Rheological studies of the worms (see below) suggest that they probably undergo a thermally triggered morphological transition to form spheres. However, confirmation would most likely require small-angle X-ray scattering studies, which are beyond the scope of this work.

Dispersion Polymerization of BzA in *n*-Dodecane or Isohexadecane. The use of *n*-heptane as a non-solvent for the PBzA block is crucial for the PISA formulation. However, this solvent is relatively volatile (bp = 98 °C) which can produce large variations in dispersion concentration and hence the data obtained from rheology experiments when they are conducted at elevated temperatures.

Therefore, *n*-heptane was replaced with either *n*-dodecane (DD) or isohexadecane (IHD), which are both much less volatile (bp >200 °C). The former solvent was of high purity (≥99%; research grade), whereas the latter solvent was technical grade (the main constituent of a 97% w/w mixture of C$_{16}$ isoparaffins).
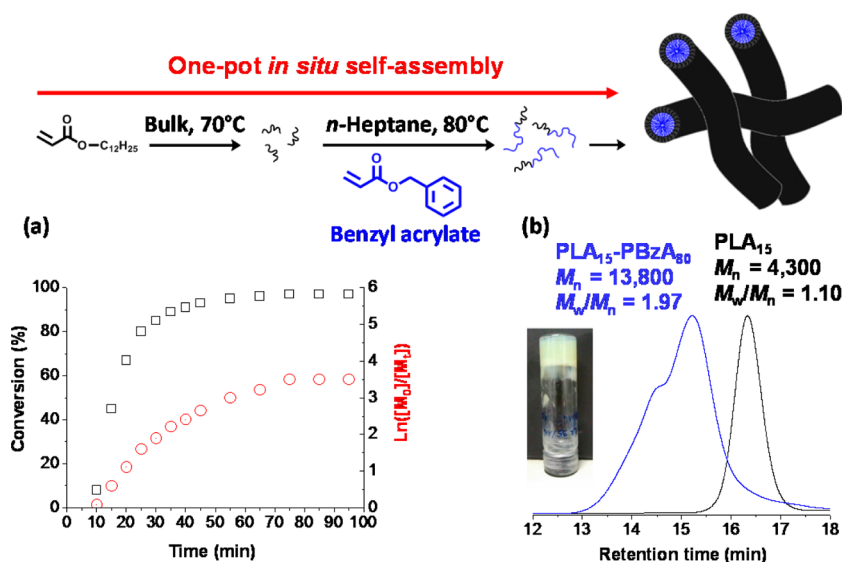
Figure 8. (a) Conversion vs time curve obtained for the synthesis of a PLA macro-CTA (target DP = 15) using a CTA/AIBN molar ratio of 5.0 at 70 °C. (b) THF GPC traces obtained for a PLA_{15} macro-CTA (97% conversion) quenched after 95 min and the corresponding PLA_{15}–$PBzA_{80}$ copolymer, which was synthesized directly without isolating the PLA macro-CTA (20% w/w in n-heptane, 80 °C for 16 h, CTA/T21S molar ratio = 5.0, >99% conversion). A digital photograph (taken at 20 °C) shows the resulting free-standing turbid gel.

A series of PLA−PBzA diblock copolymer dispersions were synthesized at 20% w/w solids in each solvent under the same conditions as those employed for n-heptane. Table 2 summarizes the molecular weight data, final monomer conversions, and physical appearance for the resulting dispersions, which are also compared in Figure S4. The data in Figure S4 suggest that changing the solvent leads to subtle differences in the precise copolymer composition required for gelation. For example, gels were obtained in IHD at a lower target PBzA DP than that required for n-heptane.

One-Pot Synthesis of PLA−PBzA Diblock Copolymers. PLA_x−$PBzA_y$ diblock copolymer nanoparticles could also be prepared using a "one-pot" protocol starting from LA monomer (see Figure 8). First, a PLA_{15} macro-CTA was synthesized via bulk polymerization targeting a DP of 15. A conversion of 97% was achieved within 1.25 h prior to quenching the polymerization. BzA monomer, T21S, and n-heptane were then added to this macro-CTA to produce a 20% w/w solids formulation (targeting PLA_{15}−$PBzA_{80}$), followed by deoxygenation and heating to 80 °C for 16 h. According to ^{1}H NMR analysis, the BzA conversion was 97%, and THF GPC analysis indicated an M_n of 13 800 g mol^{-1} and an M_w/M_n of 1.97. The blocking efficiency was relatively high (see Figure 8b), with minimal unreacted macro-CTA present in the final diblock copolymer. Overall, the molecular weight data were comparable to those obtained for a very similar copolymer synthesized using a purified PLA_{14} macro-CTA (see entry 12, Table 1). The inset digital photograph shows the turbid gel that is formed at 20 °C using the "one-pot" protocol. The analogous PLA_{14}−$PBzA_{80}$ formulation prepared by a two-step synthesis also formed a free-standing gel (see Table 1). This suggests that such "one-pot" PISA syntheses are robust and bodes well for potential industrial applications.

Rheological Characterization of PLA−PBzA Worm Gels. We have published extensively on RAFT non-polar[91,92] and aqueous[46,93] dispersion polymerization formulations, and it is now well-established that the worm phase typically forms a soft, free-standing gel. Moreover, PLMA−PBzMA worms prepared in n-dodecane were transformed into spheres upon

heating above 70 °C. This morphological transition was attributed to surface plasticization of the worm cores (as indicated by greater solvation of the PBzMA block) which resulted in a reduction in the packing parameter.[92] A similar explanation was also proposed by Pei et al.[94] for the thermoresponsive behavior of similar block copolymer worms in n-tetradecane. The worm gels reported by Fielding et al.[92] were characterized by oscillatory shear rheology, which indicated storage moduli of the order of 1000 Pa, and the worm-to-sphere transition was associated with a critical gelation temperature (CGT) of around 50 °C. In the present work, rheological studies were undertaken for PLA_{14}−$PBzA_{60}$ copolymer gels prepared at 15% w/w solids in both n-dodecane and isohexadecane. Figure S5a shows the variation in gel stiffness (represented by the storage, G', and loss, G'', moduli) with applied strain at 20 °C at a fixed angular frequency of 10 rad s^{-1}. Similar plateau regions are observed for both gels, which indicate the point where the moduli are independent of strain. G' and G'' both lie within the linear viscoelastic regime under these conditions, and hence subsequent measurements were conducted at 1% strain and 10 rad s^{-1}. The temperature dependence of the gels were subsequently examined under these conditions from 4−80−4 °C (see Figure 9).

Like the PLMA−PBzMA system described by Fielding et al.,[92] much lower gel moduli are observed at higher temperatures. However, an *additional* thermal transition is also observed at lower temperatures where the gel modulus *increases*. This results in G' falling below G'', which indicates a lower and an upper critical gelation temperature (CGT) at 12−14 °C and 67−68 °C, respectively. Similar behavior was also observed for the same diblock copolymer composition prepared in IHD, but the CGT values are shifted to higher temperatures in this case (Figure S5b). The difference between the gels is likely due to the subtle difference between the particle morphology of these samples. The turbidity of these samples is different at 20 °C (the sample in IHD is slightly milkier in appearance), suggesting a more branched worm structure has been obtained in this case according to previous studies within our group.[93] However,
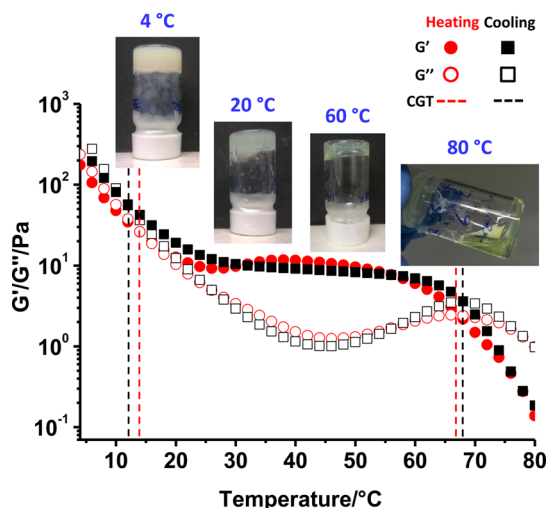
Figure 9. Variation of gel moduli (G' and G'') with temperature at an applied strain of 1.0% and an angular frequency of 10 rad s^{-1} for a PLA$_{14}$–PBzA$_{60}$ diblock copolymer prepared at 15% w/w in n-dodecane. The thermal cycle was from 4–80–4 °C, and measurements were recorded at 2 °C intervals, with 2 min being allowed for equilibration at each temperature. Digital photographs indicate the visual appearance of this copolymer dispersion at selected temperatures.

further detailed cryo-TEM or perhaps small-angle X-ray scattering (SAXS) studies would be required to confirm this hypothesis. The PLA$_{14}$–PBzA$_{60}$ gel in n-dodecane was also equilibrated at four different temperatures (see inset images for Figure 9) to provide a visual representation of the various regimes observed within the rheology data. The gel becomes much more turbid and significantly stiffer at 4 °C. At 20 °C, the gel is soft and slightly turbid but still quite resistant to mechanical

stress. Similar behavior was observed at 60 °C, although the gel is significantly less turbid at this temperature. Finally, the dispersion becomes a transparent, free-flowing liquid at 80 °C. In all cases, the rheological behavior was fully reversible. The morphologies revealed by cryo-TEM studies combined with DLS studies conducted at 4, 20, and 80 °C (see Figure S6) suggest that the changes in turbidity may be associated with a worm-to-sphere transition, while the above rheological data suggest that this transition most likely occurs at between 60 and 80 °C. This interpretation is consistent with results recently published by Fielding et al.,[92] who observed a similar order–order transition on heating a dispersion of PLMA–PBzMA worms. However, the reason for the *additional* rheological transition observed at 4 °C is as yet unclear. Cryo-TEM studies conducted at this temperature indicates the presence of a pure worm phase (see Figure S7). Thus, it is tempting to suggest that this phenomenon may be related to the T_g of 6 °C for the core-forming PBzA chains.[122] Significantly stiffer worms might be expected below this critical temperature, which might explain the rapid increase in G' (and G''). Indeed, a similar effect was reported by Bates and co-workers,[24] who found that core-cross-linked poly(ethylene oxide)–polybutadiene diblock copolymer worms formed stronger gels than the corresponding linear precursor worms. Alternatively, the significant increase in sphere-equivalent diameter indicated by DLS studies at 4 °C (see Figure S6) suggests either worm branching or clustering at this temperature. However, cryo-TEM appears to be too insensitive to corroborate either possibility, with little or no apparent change in copolymer morphology being observed (see Figure S7).

A PLA$_{14}$–PBzA$_{60}$ diblock copolymer was prepared at 40% w/w solids, and its rheological properties were characterized after dilution to 15% w/w solids. Almost identical behavior was observed for the diluted copolymer dispersion as for the equivalent dispersion prepared at 15% w/w solids (see Figure
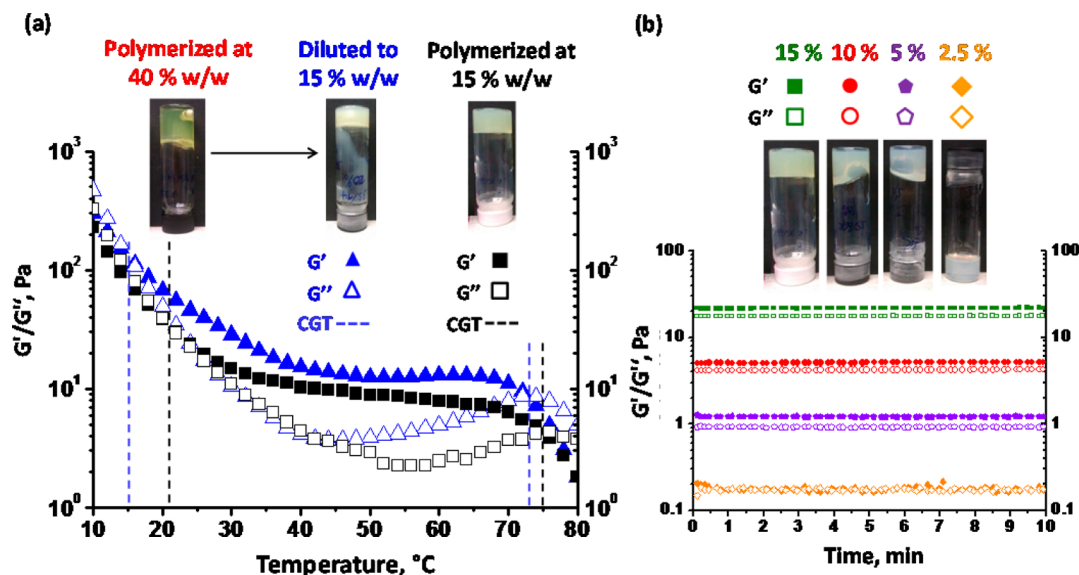
Figure 10. (a) Variation of gel modulus (G', G'') with temperature at an applied strain of 1.0% and an angular frequency of 10 rad s^{-1} for PLA$_{14}$–PBzA$_{60}$ diblock copolymers prepared in n-dodecane. The blue triangles indicate a copolymer dispersion prepared at 40% w/w solids and subsequently diluted to 15% w/w solids, whereas the black squares represent a copolymer prepared directly at 15% w/w solids. Temperature sweeps were conducted from 80 to 10 °C on the 15% w/w dispersion; measurements were taken at 2 °C intervals, with 2 min being allowed for equilibration at each temperature. Digital photographs indicate the visual appearance of the dispersions at various copolymer concentrations at 20 °C. (b) Gel moduli (G', G'') recorded over time at 20 °C for a PLA$_{14}$–PBzA$_{60}$ diblock copolymer prepared at 15% w/w solids in n-dodecane followed by serial dilution to the desired copolymer concentration. Measurements were conducted at 10 s intervals for 10 min at an applied strain of 1.0% and an angular frequency of 10 rad s^{-1}. Digital photographs indicate the visual appearance of the gels at various copolymer concentrations at 20 °C.

10a). Another important parameter is the critical gelation concentration (CGC) (see Figure 10b), which can be determined by serial dilution. At 20 °C, a free-standing gel is obtained for copolymer concentrations of ≥5% w/w solids. At 2.5% w/w solids, the dispersion remained gel-like but could no longer support its own weight in a tube inversion test, while a free-flowing liquid was observed at ≤1.25% w/w solids. Thus, the CGC is estimated to be ~2.5% w/w solids, which is in good agreement with the G'/G'' values obtained for the time-dependent gel modulus plots in Figure 10b.

■ CONCLUSIONS

A series of PLA–PBzA diblock copolymers have been prepared via RAFT dispersion polymerization in n-alkanes, with high monomer conversions being achieved for syntheses conducted at 15−40% w/w solids. Relatively high blocking efficiencies were obtained along with comparable copolymer dispersities to those reported in the literature for similar formulations.[93,94] As far as we are aware, this is the first example of an all-acrylic PISA formulation conducted in a non-polar solvent for which spherical, worm-like and vesicular particles have been obtained. Systematic variation of the copolymer concentration and the DP of the core-forming block led to a gradual increase in turbidity and a range of rheological behavior for these dispersions, including the formation of soft free-standing gels. This led to the construction of a phase diagram based on the visual appearance of the various dispersions combined with DLS data, rather than the extensive TEM studies described in earlier PISA studies. For example, observation of a gel phase was interpreted as evidence for the presence of worms, without necessarily indicating that a pure worm phase was present. This approach was adopted because the soft, film-forming nature of these low-T_g all-acrylic nanoparticles prevented conventional TEM studies. In some cases, copolymer particles were cross-linked in order to increase their T_g and so aid TEM analysis. Alternatively, selected dispersions were examined by vitrification of dilute dispersions in n-heptane using cryo-TEM. The latter approach confirmed the presence of sphere, worm, and vesicle copolymer morphologies within the phase diagram, with the presence of worms being strongly correlated with the gel phase. Rheological studies were undertaken on related worm gels prepared in either n-dodecane or isohexadecane, since these solvents are much less volatile than n-heptane. Broadly similar behavior was observed in each case but subtle differences in gel moduli and CGT were observed, which is likely due to differences in the worm contour length and degree of branching of the worm-like particles. Selected gels exhibited thermoresponsive behavior between 4 and 80 °C. Interestingly, these all-acrylic gels exhibit lower G' and G'' values than the analogous all-methacrylic gels.[92] Moreover, the former gels undergo an additional thermal transition on cooling below 15 °C which is currently believed to be related to stiffening of the worm-like particles on approaching the T_g of the PBzA block. Finally, worm gels can also be conveniently prepared at 40% w/w solids using a "one-pot" protocol starting from lauryl acrylate. On dilution, such worm gels behave similarly to worm gels prepared at 15% w/w solids. These gels exhibit a critical gelation concentration of approximately 2.5% w/w solids, which is significantly lower than the all-methacrylic worm gels previously prepared in n-alkanes.[91]

■ ASSOCIATED CONTENT

Ⓢ Supporting Information

The Supporting Information is available free of charge on the ACS Publications website at DOI: 10.1021/acs.macromol.5b02119.

> Conventional TEM images for linear $PLA_{14}–PBzA_y$ diblock copolymers and cross-linked $PLA_{14}–PBzA_y–PEGDA_6$ triblock copolymers; table displaying the controllable variation in physical appearance for $PLA_{14}–PBzA_y$ diblock copolymers upon changing the polymerization solvent from n-heptane to n-dodecane or isohexadecane; rheological characterization of gel stiffness vs strain % for $PLA_{14}–PBzA_{60}$ 15% w/w dispersions at 20 °C in n-dodecane and isohexadecane and temperature sweep for $PLA_{14}–PBzA_{60}$ diblock copolymer synthesized at 15% w/w in isohexadecane; DLS data obtained for $PLA_{14}–PBzA_{60}$ copolymer gel in n-dodecane at 4, 20, and 80 °C and cryo-TEM images obtained for $PLA_{14}–PBzA_{70}$ diblock copolymer prepared in n-heptane at 4 and 20 °C (PDF).

■ AUTHOR INFORMATION

Corresponding Author

*E-mail s.p.armes@shef.ac.uk (S.P.A.).

Notes

The authors declare no competing financial interest.

■ ACKNOWLEDGMENTS

■ REFERENCES

(1) Tadros, T. *Adv. Colloid Interface Sci.* **2009**, *147−148*, 281−299.
(2) Van Herk, A. M.; Monteiro, M. Heterogeneous Systems. In *Handbook of Radical Polymerization*; John Wiley & Sons, Inc.: Hoboken, NJ, 2003; pp 301−331.
(3) Ober, C. K.; Lok, K. P. *Macromolecules* **1987**, *20*, 268−273.
(4) Lok, K. P.; Ober, C. K. *Can. J. Chem.* **1985**, *63*, 209−216.
(5) Corner, T. *Colloids Surf.* **1981**, *3*, 119−129.
(6) Shen, S.; Sudol, E. D.; El-Aasser, M. S. *J. Polym. Sci., Part A: Polym. Chem.* **1993**, *31*, 1393−1402.
(7) Richez, A. P.; Yow, H. N.; Biggs, S.; Cayre, O. J. *Prog. Polym. Sci.* **2013**, *38*, 897−931.
(8) Horák, D. *Acta Polym.* **1996**, *47*, 20−28.
(9) Riess, G.; Labbe, C. *Macromol. Rapid Commun.* **2004**, *25*, 401−435.
(10) Kawaguchi, H. *Prog. Polym. Sci.* **2000**, *25*, 1171−1210.
(11) Asua, J. M. Dispersions, N. A. S. I. o. R. A. i. P. *Polymeric Dispersions: Principles and Applications*; Kluwer Academic: Dordrecht, 1997; p *xix*, 565 pp.
(12) Arshady, R. *Biomaterials* **1993**, *14*, 5−15.
(13) Kawaguchi, S.; Ito, K. Dispersion Polymerization. In *Polymer Particles*; Okubo, M., Ed.; Springer-Verlag: New York, 2005; Vol. *175*, pp 299−328.
(14) Price, C. *Pure Appl. Chem.* **1983**, *55*, 1563−1572.
(15) Discher, D. E.; Eisenberg, A. *Science* **2002**, *297*, 967−973.
(16) Discher, B. M.; You-Yeon, W.; Ege, D. S.; Lee, J. C. M.; Bates, F. S.; Discher, D. E.; Hammer, D. A. *Science* **1999**, *284*, 1143−1146.
(17) Xu, R.; Winnik, M. A.; Hallett, F. R.; Riess, G.; Croucher, M. D. *Macromolecules* **1991**, *24*, 87−93.
(18) Zhang, L.; Yu, K.; Eisenberg, A. *Science* **1996**, *272*, 1777−1779.
(19) Zhang, L.; Eisenberg, A. *Science* **1995**, *268*, 1728−1731.
(20) Mai, Y.; Eisenberg, A. *Chem. Soc. Rev.* **2012**, *41*, 5969−5985.

(21) Yang, Z.; Pickard, S.; Deng, N.-J.; Barlow, R. J.; Attwood, D.; Booth, C. *Macromolecules* **1994**, *27*, 2371−2379.

(22) Booth, C.; Attwood, D. *Macromol. Rapid Commun.* **2000**, *21*, 501−527.

(23) Jain, S.; Bates, F. S. *Macromolecules* **2004**, *37*, 1511−1523.

(24) Won, Y.-Y.; Davis, H. T.; Bates, F. S. *Science* **1999**, *283*, 960−963.

(25) Blanazs, A.; Armes, S. P.; Ryan, A. J. *Macromol. Rapid Commun.* **2009**, *30*, 267−277.

(26) Zhang, L.; Eisenberg, A. *Polym. Adv. Technol.* **1998**, *9*, 677−699.

(27) Arifin, D. R.; Palmer, A. F. *Biomacromolecules* **2005**, *6*, 2172−2181.

(28) Brannan, A. K.; Bates, F. S. *Macromolecules* **2004**, *37*, 8816−8819.

(29) Ghoroghchian, P. P.; Li, G.; Levine, D. H.; Davis, K. P.; Bates, F. S.; Hammer, D. A.; Therien, M. J. *Macromolecules* **2006**, *39*, 1673−1675.

(30) Lomas, H.; Massignani, M.; Abdullah, K. A.; Canton, I.; Lo Presti, C.; MacNeil, S.; Du, J.; Blanazs, A.; Madsen, J.; Armes, S. P.; Lewis, A. L.; Battaglia, G. *Faraday Discuss.* **2008**, *139*, 143−159.

(31) Hawker, C. J.; Bosman, A. W.; Harth, E. *Chem. Rev.* **2001**, *101*, 3661−3688.

(32) Wang, J.-S.; Matyjaszewski, K. *J. Am. Chem. Soc.* **1995**, *117*, 5614−5615.

(33) Kato, M.; Kamigaito, M.; Sawamoto, M.; Higashimura, T. *Macromolecules* **1995**, *28*, 1721−1723.

(34) Chiefari, J.; Chong, Y. K.; Ercole, F.; Krstina, J.; Jeffery, J.; Le, T. P. T.; Mayadunne, R. T. A.; Meijs, G. F.; Moad, C. L.; Moad, G.; Rizzardo, E.; Thang, S. H. *Macromolecules* **1998**, *31*, 5559−5562.

(35) Lowe, A. B.; McCormick, C. L. *Prog. Polym. Sci.* **2007**, *32*, 283−351.

(36) Qiu, J.; Charleux, B.; Matyjaszewski, K. *Prog. Polym. Sci.* **2001**, *26*, 2083−2134.

(37) Cunningham, M. F. *Prog. Polym. Sci.* **2008**, *33*, 365−398.

(38) Boyer, C.; Stenzel, M. H.; Davis, T. P. *J. Polym. Sci., Part A: Polym. Chem.* **2011**, *49*, 551−595.

(39) Mertoglu, M.; Garnier, S.; Laschewsky, A.; Skrabania, K.; Storsberg, J. *Polymer* **2005**, *46*, 7726−7740.

(40) McCormick, C. L.; Sumerlin, B. S.; Lokitz, B. S.; Stempka, J. E. *Soft Matter* **2008**, *4*, 1760−1773.

(41) Pochan, D. J.; Chen, Z.; Cui, H.; Hales, K.; Qi, K.; Wooley, K. L. *Science* **2004**, *306*, 94−97.

(42) Wan, W.-M.; Pan, C.-Y. *Polym. Chem.* **2010**, *1*, 1475−1484.

(43) Chaduc, I.; Zhang, W.; Rieger, J.; Lansalot, M.; D'Agosto, F.; Charleux, B. *Macromol. Rapid Commun.* **2011**, *32*, 1270−1276.

(44) Perrier, S.; Takolpuckdee, P. *J. Polym. Sci., Part A: Polym. Chem.* **2005**, *43*, 5347−5393.

(45) Ruzette, A.-V.; Tencé-Girault, S.; Leibler, L.; Chauvin, F.; Bertin, D.; Guerret, O.; Gérard, P. *Macromolecules* **2006**, *39*, 5804−5814.

(46) Charleux, B.; Delaittre, G.; Rieger, J.; D'Agosto, F. *Macromolecules* **2012**, *45*, 6753−6765.

(47) Warren, N. J.; Armes, S. P. *J. Am. Chem. Soc.* **2014**, *136*, 10174−10185.

(48) Du, J.; O'Reilly, R. K. *Soft Matter* **2009**, *5*, 3544−3561.

(49) Holder, S. J.; Sommerdijk, N. A. J. M. *Polym. Chem.* **2011**, *2*, 1018−1028.

(50) Theato, P. *J. Polym. Sci., Part A: Polym. Chem.* **2008**, *46*, 6677−6687.

(51) Stenzel, M. H. *Chem. Commun.* **2008**, 3486−3503.

(52) Matyjaszewski, K.; Gnanou, Y.; Leibler, L. *Macromolecular Engineering: Precise Synthesis, Materials Properties, Applications*; Wiley-VCH Verlag GmbH & Co. KGaA: Weinheim, 2007; Vol. 4, pp 2181−2224.

(53) Kessel, S.; Truong, N. P.; Jia, Z.; Monteiro, M. J. *J. Polym. Sci., Part A: Polym. Chem.* **2012**, *50*, 4879−4887.

(54) Manguian, M.; Save, M.; Charleux, B. *Macromol. Rapid Commun.* **2006**, *27*, 399−404.

(55) Stoffelbach, F.; Tibiletti, L.; Rieger, J.; Charleux, B. *Macromolecules* **2008**, *41*, 7850−7856.

(56) Zhang, W.; Charleux, B.; Cassagnau, P. *Macromolecules* **2012**, *45*, 5273−5280.

(57) Zhang, W.; D'Agosto, F.; Boyron, O.; Rieger, J.; Charleux, B. *Macromolecules* **2011**, *44*, 7584−7593.

(58) Zhang, W.; D'Agosto, F.; Boyron, O.; Rieger, J.; Charleux, B. *Macromolecules* **2012**, *45*, 4075−4084.

(59) Zhang, W.; D'Agosto, F.; Dugas, P.-Y.; Rieger, J.; Charleux, B. *Polymer* **2013**, *54*, 2011−2019.

(60) Zhang, X.; Rieger, J.; Charleux, B. *Polym. Chem.* **2012**, *3*, 1502−1509.

(61) Blanazs, A.; Madsen, J.; Battaglia, G.; Ryan, A. J.; Armes, S. P. *J. Am. Chem. Soc.* **2011**, *133*, 16581−16587.

(62) Blanazs, A.; Ryan, A. J.; Armes, S. P. *Macromolecules* **2012**, *45*, 5099−5107.

(63) Blanazs, A.; Verber, R.; Mykhaylyk, O. O.; Ryan, A. J.; Heath, J. Z.; Douglas, C. W. I.; Armes, S. P. *J. Am. Chem. Soc.* **2012**, *134*, 9741−9748.

(64) Grazon, C.; Rieger, J.; Sanson, N.; Charleux, B. *Soft Matter* **2011**, *7*, 3482−3490.

(65) An, Z.; Shi, Q.; Tang, W.; Tsung, C.-K.; Hawker, C. J.; Stucky, G. D. *J. Am. Chem. Soc.* **2007**, *129*, 14493−14499.

(66) Yan, L.; Tao, W. *Polymer* **2010**, *51*, 2161−2167.

(67) Figg, C. A.; Simula, A.; Gebre, K. A.; Tucker, B. S.; Haddleton, D.; Sumerlin, B. S. *Chem. Sci.* **2015**, *6*, 1230−1236.

(68) Cunningham, V. J.; Ratcliffe, L. P. D.; Blanazs, A.; Warren, N. J.; Smith, A. J.; Mykhaylyk, O. O.; Armes, S. P. *Polym. Chem.* **2014**, *5*, 6307−6317.

(69) Ratcliffe, L. P. D.; Blanazs, A.; Williams, C. N.; Brown, S. L.; Armes, S. P. *Polym. Chem.* **2014**, *5*, 3643−3655.

(70) Ratcliffe, L. P. D.; Ryan, A. J.; Armes, S. P. *Macromolecules* **2013**, *46*, 769−777.

(71) Lovett, J. R.; Warren, N. J.; Ratcliffe, L. P. D.; Kocik, M. K.; Armes, S. P. *Angew. Chem., Int. Ed.* **2015**, *54*, 1279−1283.

(72) Cai, W.; Wan, W.; Hong, C.; Huang, C.; Pan, C.-Y. *Soft Matter* **2010**, *6*, 5554−5561.

(73) Huang, C.-Q.; Pan, C.-Y. *Polymer* **2010**, *51*, 5115−5121.

(74) Semsarilar, M.; Jones, E. R.; Blanazs, A.; Armes, S. P. *Adv. Mater.* **2012**, *24*, 3378−3382.

(75) Jones, E. R.; Semsarilar, M.; Blanazs, A.; Armes, S. P. *Macromolecules* **2012**, *45*, 5091−5098.

(76) McKee, J. R.; Ladmiral, V.; Niskanen, J.; Tenhu, H.; Armes, S. P. *Macromolecules* **2011**, *44*, 7692−7703.

(77) Lee, J. M.; Lee, B. H.; Choe, S. *Polymer* **2006**, *47*, 3838−3844.

(78) Saikia, P. J.; Lee, J. M.; Lee, K.; Choe, S. *J. Polym. Sci., Part A: Polym. Chem.* **2008**, *46*, 872−885.

(79) Song, J.-S.; Winnik, M. A. *Macromolecules* **2006**, *39*, 8318−8325.

(80) Wan, W.-M.; Sun, X.-L.; Pan, C.-Y. *Macromol. Rapid Commun.* **2010**, *31*, 399−404.

(81) Zehm, D.; Ratcliffe, L. P. D.; Armes, S. P. *Macromolecules* **2013**, *46*, 128−139.

(82) Pei, Y.; Dharsana, N. C.; van Hensbergen, J. A.; Burford, R. P.; Roth, P. J.; Lowe, A. B. *Soft Matter* **2014**, *10*, 5787−5796.

(83) Semsarilar, M.; Penfold, N. J. W.; Jones, E. R.; Armes, S. P. *Polym. Chem.* **2015**, *6*, 1751−1757.

(84) Zhao, W.; Gody, G.; Dong, S.; Zetterlund, P. B.; Perrier, S. *Polym. Chem.* **2014**, *5*, 6990−7003.

(85) Xu, Y.; Li, Y.; Cao, X.; Chen, Q.; An, Z. *Polym. Chem.* **2014**, *5*, 6244−6255.

(86) Tan, J.; Zhao, G.; Lu, Y.; Zeng, Z.; Winnik, M. A. *Macromolecules* **2014**, *47*, 6856−6866.

(87) Karagoz, B.; Esser, L.; Duong, H. T.; Basuki, J. S.; Boyer, C.; Davis, T. P. *Polym. Chem.* **2014**, *5*, 350−355.

(88) Gonzato, C.; Semsarilar, M.; Jones, E. R.; Li, F.; Krooshof, G. J. P.; Wyman, P.; Mykhaylyk, O. O.; Tuinier, R.; Armes, S. P. *J. Am. Chem. Soc.* **2014**, *136*, 11100−11106.

(89) Zheng, G.; Pan, C. *Macromolecules* **2006**, *39*, 95−102.

(90) Ji, W.; Yan, J.; Chen, E.; Li, Z.; Liang, D. *Macromolecules* **2008**, *41*, 4914−4919.

(91) Fielding, L. A.; Derry, M. J.; Ladmiral, V.; Rosselgong, J.; Rodrigues, A. M.; Ratcliffe, L. P. D.; Sugihara, S.; Armes, S. P. *Chemical Science* **2013**, *4*, 2081−2087.

(92) Fielding, L. A.; Lane, J. A.; Derry, M. J.; Mykhaylyk, O. O.; Armes, S. P. *J. Am. Chem. Soc.* **2014**, *136*, 5790−5798.

(93) Verber, R.; Blanazs, A.; Armes, S. P. *Soft Matter* **2012**, *8*, 9915−9922.

(94) Pei, Y.; Thurairajah, L.; Sugita, O. R.; Lowe, A. B. *Macromolecules* **2015**, *48*, 236−244.

(95) Steward, P. A.; Hearn, J.; Wilkinson, M. C. *Adv. Colloid Interface Sci.* **2000**, *86*, 195−267.

(96) Czech, Z.; Pełech, R. *Prog. Org. Coat.* **2009**, *65*, 84−87.

(97) Ahmad, N. M.; Heatley, F.; Britton, D.; Lovell, P. A. *Macromol. Symp.* **1999**, *143*, 231−241.

(98) Heatley, F.; Lovell, P. A.; Yamashita, T. *Macromolecules* **2001**, *34*, 7636−7641.

(99) Ahmad, N. M.; Charleux, B.; Farcet, C.; Ferguson, C. J.; Gaynor, S. G.; Hawkett, B. S.; Heatley, F.; Klumperman, B.; Konkolewicz, D.; Lovell, P. A.; Matyjaszewski, K.; Venkatesh, R. *Macromol. Rapid Commun.* **2009**, *30*, 2002−2021.

(100) Chaduc, I.; Crepet, A.; Boyron, O.; Charleux, B.; D'Agosto, F.; Lansalot, M. *Macromolecules* **2013**, *46*, 6013−6023.

(101) Boissé, S.; Rieger, J.; Pembouong, G.; Beaunier, P.; Charleux, B. *J. Polym. Sci., Part A: Polym. Chem.* **2011**, *49*, 3346−3354.

(102) Boissé, S.; Rieger, J.; Belal, K.; Di-Cicco, A.; Beaunier, P.; Li, M.-H.; Charleux, B. *Chem. Commun.* **2010**, *46*, 1950−1952.

(103) Delaittre, G.; Dire, C.; Rieger, J.; Putaux, J.-L.; Charleux, B. *Chem. Commun.* **2009**, *20*, 2887−2889.

(104) Chaduc, I.; Girod, M.; Antoine, R.; Charleux, B.; D'Agosto, F.; Lansalot, M. *Macromolecules* **2012**, *45*, 5881−5893.

(105) Chenal, M.; Bouteiller, L.; Rieger, J. *Polym. Chem.* **2013**, *4*, 752−762.

(106) Ferguson, C. J.; Hughes, R. J.; Nguyen, D.; Pham, B. T. T.; Gilbert, R. G.; Serelis, A. K.; Such, C. H.; Hawkett, B. S. *Macromolecules* **2005**, *38*, 2191−2204.

(107) Rieger, J.; Zhang, W.; Stoffelbach, F.; Charleux, B. *Macromolecules* **2010**, *43*, 6302−6310.

(108) Qiu, Q.; Liu, G.; An, Z. *Chem. Commun.* **2011**, *47*, 12685−12687.

(109) Rieger, J.; Osterwinter, G.; Bui, C.; Stoffelbach, F.; Charleux, B. *Macromolecules* **2009**, *42*, 5518−5525.

(110) Rieger, J.; Stoffelbach, F.; Bui, C.; Alaimo, D.; Jérôme, C.; Charleux, B. *Macromolecules* **2008**, *41*, 4065−4068.

(111) Liu, G.; Qiu, Q.; An, Z. *Polym. Chem.* **2012**, *3*, 504−513.

(112) Liu, G.; Qiu, Q.; Shen, W.; An, Z. *Macromolecules* **2011**, *44*, 5237−5245.

(113) He, W.-D.; Sun, X.-L.; Wan, W.-M.; Pan, C.-Y. *Macromolecules* **2011**, *44*, 3358−3365.

(114) Bathfield, M.; D'Agosto, F.; Spitz, R.; Charreyre, M.-T.; Pichot, C.; Delair, T. *Macromol. Rapid Commun.* **2007**, *28*, 1540−1545.

(115) Zhang, X.; Boissé, S.; Bui, C.; Albouy, P.-A.; Brulet, A.; Li, M.-H.; Rieger, J.; Charleux, B. *Soft Matter* **2012**, *8*, 1130−1141.

(116) Charbonnier, A.; Brochon, C.; Cloutet, E.; Navarro, C.; Hadziioannou, G. *J. Polym. Sci., Part A: Polym. Chem.* **2013**, *51*, 4608−4617.

(117) Houillot, L.; Bui, C.; Farcet, C. l.; Moire, C.; Raust, J.-A.; Pasch, H.; Save, M.; Charleux, B. *ACS Appl. Mater. Interfaces* **2010**, *2*, 434−442.

(118) Houillot, L.; Bui, C.; Save, M.; Charleux, B.; Farcet, C.; Moire, C.; Raust, J.-A.; Rodriguez, I. *Macromolecules* **2007**, *40*, 6500−6509.

(119) Moad, G.; Rizzardo, E.; Thang, S. H. *Aust. J. Chem.* **2009**, *62*, 1402−1472.

(120) Moad, G.; Barner-Kowollik, C. The Mechanism and Kinetics of the RAFT Process: Overview, Rates, Stabilities, Side Reactions, Product Spectrum and Outstanding Challenges. In *Handbook of RAFT Polymerization*; Wiley-VCH Verlag GmbH & Co. KGaA: Weinheim, 2008; pp 51−104.

(121) Veloso, A.; Garcia, W.; Agirre, A.; Ballard, N.; Ruiperez, F.; de la Cal, J. C.; Asua, J. M. *Polym. Chem.* **2015**, *6*, 5437−5450.

(122) Liu, W.; Cao, C. *Colloid Polym. Sci.* **2009**, *287*, 811−818.

(123) Cui, H.; Hodgdon, T. K.; Kaler, E. W.; Abezgauz, L.; Danino, D.; Lubovsky, M.; Talmon, Y.; Pochan, D. J. *Soft Matter* **2007**, *3*, 945−955.

(124) Putaux, J.-L.; Minatti, E.; Lefebvre, C.; Borsali, R.; Schappacher, M.; Deffieux, A. *Faraday Discuss.* **2005**, *128*, 163−178.

(125) Mihut, A. M.; Chiche, A.; Drechsler, M.; Schmalz, H.; Di Cola, E.; Krausch, G.; Ballauff, M. *Soft Matter* **2009**, *5*, 208−213.

(126) Mihut, A. M.; Drechsler, M.; Möller, M.; Ballauff, M. *Macromol. Rapid Commun.* **2010**, *31*, 449−453.